Hybrid Nanocoolant for Enhanced Heat Transfer Performance in Vehicle Cooling System

Hong Wei Xian[a],* , Nor Azwadi Che Sidik [a],* , R. Saidur [b,c]

[a] Malaysia – Japan International Institute of Technology (MJIIT), Universiti Teknologi Malaysia Kuala Lumpur, Jalan Sultan Yahya Petra (Jalan Semarak), 54100 Kuala Lumpur, Malaysia

[b] Research Centre for Nano-Materials and Energy Technology (RCNMET), School of Engineering and Technology, Sunway University, No. 5, Jalan Universiti, Bandar Sunway, 47500 Petaling Jaya, Selangor, Malaysia

[c] Department of Engineering, Lancaster University, LA1 4YW, United Kingdom

Abstract

An enormous amount of heat generated from a vehicle engine could be removed fractionally by using a radiator. The struggle to maintain efficient heat exchange in a vehicle cooling system is arduous as both active and passive methods require time to catch up with high-power engine technologies. This study reported the heat transfer performance of a novel hybrid nanocoolant with various mixing ratios. The hybrid nanocoolant consisted of carboxyl-functionalised graphene nanoplatelets (CGnP) and titanium dioxide (TiO_2) nanoparticles in a mixture of distilled water and ethylene glycol. The thermal performance of the hybrid nanocoolant was conducted using a test rig equipped with a crossflow type radiator. The effect of different hybrid mixing ratios, Reynolds number, and air inlet velocity on heat transfer performance was studied. The Nusselt number obtained with distilled water and base coolant was close to the Dehghandokht's and Shah-London's correlations. When CGnP-TiO_2 (70:30) with 0.1 wt.% concentration was mixed into the base coolant, 4.94%, 35.87%, and 20.48% of maximum increments were observed for Nusselt number, overall heat transfer coefficient, and effectiveness of radiator, respectively. The maximum error in estimating heat transfer performance using proposed correlations was less than 8%. It can be concluded that hybrid nanocoolant with different mixing ratios significantly affects heat transfer performance. This characteristic is vital for determining the best possible attributes in various nanocomposite combinations.

Nomenclature

List of Abbreviation

Al_2O_3	Aluminium oxide
CGnP	Carboxyl-functionalized graphene nanoplatelets
CNT	Carbon nanotube
Co_3O_4	Cobalt oxide
DW	Distilled water

EG	Ethylene glycol
Fe_3O_4	Iron oxide
GnP	Graphene nanoplatelet
LMTD	Log mean temperature difference
Nu	Nusselt number
OHTC	Overall heat transfer coefficient
Pr	Prandtl number
Re	Reynolds number
TiO_2	Titanium dioxide
W	Water
γ-Al_2O_3	Gamma aluminium oxide

List of Symbols

A	Area
C_p	Specific heat capacity
D	Diameter
h	Height
k	Thermal conductivity
l	Length
$\dot{m}$	Mass flow rate
n	Number
$\dot{Q}$	Heat transfer rate
T	Temperature
U	Overall heat transfer coefficient
u	Uncertainty of variable
vol.%	Volume concentration
wt.%	Weightage concentration
ε	Effectiveness of radiator
ρ	Density
μ	Viscosity

List of Subscripts

Ave	Average
b	Bulk
bc	Base coolant
CF	Correction factor
est	Estimated performance
hb	Heat balance
nc	Nanocoolant

1.0 Introduction

Nowadays, it is still common to see overheated vehicles breaking down on the roadside. The primary causes of engine overheating are a worn-out radiator, an eroded water pump, and inefficient coolant. Overheating could cause damage to various parts of the vehicle, such as warping the cylinder head, deformation of the radiator hose, and eventually, a vehicle breakdown. There is still much room for improvement, and various techniques for enhancing the performance of vehicle cooling systems have been reported. Generally, there are three methods to improve cooling efficiency: passive cooling, active cooling, or a combination of the two [1]. A passive approach is environmentally and economically friendly, such as changing radiator body material, fin configuration and putting inserts into the flow passage.

On the other hand, the active method mainly involves external power consumption for improved cooling capability, such as installing a cooling fan to remove excess heat or using coolant (water and antifreeze). Both methods are widely used in every vehicle to maximise the efficiency of heat transfer. However, these methods have limitations while retaining the same system size, space, or input power. Therefore, to further improve the efficiency of the passive cooling technique, an additive such as nanoparticles (< 100 nm) for coolant could be of great potential, as this technology has been shown to significantly enhance heat transfer performance in various systems [2-4].

Solids are known to transfer heat much better than liquids due to their intrinsic high thermal conductivity. Hence, many studies have discovered the thermal characteristics of an innovative mixture composed of liquid and nano-sized solid particles. In 1995, the solid-liquid mixture was named 'nanofluid' by Choi and Eastman [5]. These nanoparticles' high total surface area promotes even more heat exchange between fluid molecules and solid particles. The intriguing properties of nanofluid had shown a remarkable performance in most heat transfer applications, with only a few studies reporting performance deterioration. Hence, some experimental works on testing nanofluids in vehicle radiators

was reviewed. Consequently, the terms 'nanofluid' and 'base fluid' are rephrased 'nanocoolant' and 'base coolant', respectively.

Gulhane et al. [6] tested water-based alumina nanocoolant on a fan-cooled radiator test rig. The parameters altered were nanoparticles concentration (0.1 vol.% to 0.4 vol.%), flow rate (2 to 5 L/min), and inlet temperature (50, 60, and 70 °C). 45.87% increment in the heat transfer coefficient was acquired compared to the base coolant's 0.4 vol.% aluminium oxide (Al_2O_3) nanoparticles. Although their statistical analysis showed clear outliers among the few data points, the authors proposed a linear regression. The proposed correlation, with a 3% of maximum deviation, did not look promising. Sheikhzadeh et al. [7] performed a laminar flow study on Al_2O_3-water/ethylene glycol (W/EG) (40:60) and set 9, 11, and 13 L/min of coolant flow rate passing through a flat tube radiator. At a flow rate of 13 L/min, 0.012 vol.% alumina nanocoolant enhanced the Nusselt number by about 9% compared to the base coolant.

The Reynolds number was much lower than the previous study [6], the Reynolds number was much lower, although the coolant flow rate doubled. This situation is due to the different Nusselt number computations based on either all tubes or a single tube on the radiator, hence the main reason why some studies reported turbulent flow even at low coolant flow rates. An overall heat transfer coefficient (OHTC) should be reported to describe the heat transfer performance in a vehicle radiator instead of the Nusselt number. Alumina was observed to improve the Nusselt number of W/EG (50:50) by 28.47% with a concentration of 0.8 vol.% at 4 L/min of coolant flow rate using the same type of radiator [8]. By fixing the pumping power, the nanocoolant was able to reduce the total surface area of the radiator up to 58.34% compared to the conventional coolant. The maximum deviation (25%) displayed by several data points predicted using their proposed correlation could be due to the high uncertainty (18.9%) calculated from equipment and sensors. This situation may perplex others in determining the precise factor affecting heat transfer performance.

Meanwhile, Elsaid [9] showed that W/EG with cobalt oxide (Co_3O_4) outperformed Al_2O_3. The Nusselt number and radiator effectiveness increased with Reynolds number and nanoparticle concentration in the crossflow radiator test rig. However, increasing coolant inlet temperature and EG ratio in the coolant causes heat transfer to deteriorate. At 0.1 m^3/s of coolant flow rate and 0.1 vol.% nanoparticles, the Nusselt number of Co_3O_4 nanocoolant was 16.7% and 31.8% higher than Al_2O_3 nanocoolant and base coolant, respectively, at 90 °C of inlet temperature. Despite this, when friction factor was considered, lower nanoparticle concentrations showed a higher performance index for both Al_2O_3 and

Co_3O_4 nanocoolants. This trend is due to the high viscosity (pumping power) caused by a tenfold increase in nanoparticles concentration from 0.02 vol.%.

Jagadishwar and Sudhakar [10] investigated the heat transfer performance of titanium dioxide (TiO_2) nanocoolant (0.1%, 0.2% and 0.35% of volume concentration) from 6 to 16 L/min on a crossflow type radiator. They obtained a heat transfer inclination of 42.5% with only 0.35 wt.% of TiO_2 nanoparticles added to water/propylene glycol (60:40). Devireddy et al. [11] demonstrated the performance of TiO_2 nanocoolant at different concentrations using a crossflow heat exchanger. Coolant inlet temperature showed a minimal impact on Nusselt number when compared to other parameters. They obtained a 35% heat transfer improvement using 0.5 vol.% of TiO_2 nanocoolant and proposed that Brownian motion, rather than the intrinsic thermophysical properties of nanoparticles, might be the main contributor to the enhancement. However, correlations were used to compute all thermophysical properties of the nanocoolant. The study did not consider the stability and actual properties of nanocoolant after adding surfactant. However, these two properties have been proven to impact the performance of nanocoolants [12-14].

Meanwhile, Tafakhori et al. [15] showed that 0.1 vol.% iron oxide (Fe_3O_4) nanoparticles added to the water could reduce the coolant outlet temperature at the radiator by 21%. Although 0.1 vol.% nanocoolant demonstrated the highest heat transfer rate, the maximum thermal conductivity enhancement (550.73%) was observed at 0.9 vol.%. This phenomenon revealed that thermal conductivity was not the only factor that affects heat transfer performance. Moreover, the high concentration of nanoparticles significantly increased pressure drops; hence an optimum concentration was proposed.

The effectiveness of a multi-walled carbon nanotube (MWCNT) nanocoolant in an air-cooled radiator was determined by Oliveira et al. [16]. The experiment's constant parameter was the airflow rate of 0.175 kg/s, and the inlet temperature was increased from 50 to 80 °C. The flow rate of the hot fluid, which was cooled by air, ranged from 30 g/s to 70 g/s. Heat transfer deterioration of up to 17% was observed at 0.16 wt.% MWCNT-water, while a lower concentration nanocoolant (0.5 wt.%) showed heat transfer performance was comparable to water. In contrast to most studies, distilled water presented a higher heat transfer rate than all nanocoolants used in their work. It is primarily due to their low nanocoolant's stability.

Subsequently, the performance of TiO_2 and Al_2O_3 dispersed in W/EG was compared by Said et al. [17]. They found an optimum coolant flow rate in the system, where the Nusselt number did not increase after a certain limit due to inadequate time for proper heat transfer. Alumina nanocoolant

outperformed titania nanocoolant. At 1 L/min of flow rate and 0.3 vol.% of nanoparticles, Nusselt number enhancements of 24.21% and 14.99% were observed for alumina and titania nanocoolants, respectively, compared to the base coolant. At 70 °C, both alumina and titania nanocoolant showed pressure drop reductions of up to 14.74% and 10.03%, respectively, under the same testing conditions. Performance evaluation criterion (PEC) of 0.3 vol.% Al_2O_3 and 0.3 vol.% TiO_2 at 1 L/min were 131% and 122%, respectively. Based on their findings, nanocoolant is favourable compared to the conventional coolant.

Several studies have also shown that hybrid nanocoolants outperform mono-nanocoolant. A hybrid nanocoolant consists of two or more types of nanoparticles mixed in with the base coolant. Palaniappan and Ramasamy [18] conducted a study whereby they mixed a mixture of several components (alumina, ferric oxide, titania, magnesia, silica and calcium oxide, sodium oxide, sulphur trioxide, and potassium oxide) made up as fly ash in a mixture of deionised water and ethylene glycol (DI/EG). Their setup composed a six-cylinder internal combustion engine and a crossflow type radiator. Based on both energy and exergy analyses, the optimised concentration (2 vol.%) of fly ash could enhance the OHTC of base coolant by up to 21% at Reynolds number of 8,000.

The base coolant OHTC increased by about 11% and deteriorated around 11% when 2.0 vol.% of TiO_2-Ag and TiO_2 nanoparticles were added in 50:50 W/EG, respectively. Due to higher thermal conductivity, pure TiO_2 nanocoolant was reported to achieve a performance factor of only < 1 when doped with silver nanoparticles. On the other hand, the nanocoolant with TiO_2 doped with Cu nanoparticles showed no heat transfer improvement, indicating the presence of a synergistic effect between different nanoparticles [19].

On an air-cooled radiator, Kumar and Sahoo [20] compared two different types of hybrid nanocoolant. They discovered that Al_2O_3-graphene nanoplatelet (GnP) nanocoolant performed 2.94% better than Al_2O_3-carbon nanotube (CNT) nanocoolant. They concluded that the performance difference was due to the configuration of the carbon allotropes as GnP is a planar form of carbon nanotubes with multilayers. Later, Sahoo [21] expanded on the research by mixing the three nanoparticles in water to create an Al_2O_3-GnP-CNT trihybrid nanocoolant.

Based on their scanning electron microscope (SEM) images, Al_2O_3 nanoparticles were decorated on CNTs and intercalated between GnP sheets, which could significantly increase the effective surface area for better heat transfer. When the nanoparticles concentration was increased from 1 to 3 vol.% at Reynolds number of 20,270, the heat transfer rate and performance index improved by 22.34% and deteriorated by 26.77%, respectively. It can be inferred that the trihybrid nanocoolant's high pumping

power is much higher than its heat transfer enhancement; hence it is not recommended as a coolant substitute. Other studies on the heat transfer performance of nanocoolants in various configurations of the radiator are tabulated in Table 1.

Table 1. Some previous studies on heat transfer performance of nanocoolant in different configurations of heat exchanger

Type of radiator	Nanoparticles	Base coolant	Increment obtained compared to base coolant	Ref
Crossflow	0.06 vol.% Al_2O_3-CuO	W/EG (60:40)	Heat transfer coefficient (23.2%)	[22]
	0.65 vol.% Fe_2O_3	Water	OHTC (13%)	[23]
	0.5 vol.% Al_2O_3	DW/EG (50:50)	Smaller radiator frontal surface area (15%)	[24]
Shell and tube heat exchanger	0.3 vol.% γ-Al_2O_3	Water	Nusselt number (29.8%) Overall heat transfer coefficient (19.1%)	[25]
	4 vol.% Al_2O_3 (20 nm)	Water	Average heat transfer coefficient (11.94%)	[26]
	1 vol.% Al_2O_3 (20 nm)	Water	Nusselt number (20%) Friction factor (6%)	[27]
Double tube heat exchanger	1 vol.% TiO_2 (21 nm)	Water	Heat transfer coefficient (26%) Pressure drops (19%)	[28]
	0.15 vol.% γ-Al_2O_3 (20 nm)	Water	Heat transfer coefficient (25%)	[29]
Air-cooled heat exchanger	0.02 wt.% hybrid carbon (20-30 nm)	Water	Heat exchange capacity (13%) System efficiency factor (11.7%)	[30]
Double pipe U-bend heat exchanger	0.06 vol.% Fe_3O_4 (36 nm)	Water	Heat transfer enhancement (14.7%) Effectiveness (2.4%)	[31]
Counterflow heat exchanger	0.45 vol.% Ag (30-90 nm)	Water/EG (70:30)	Convective heat transfer coefficient (42%)	[32]
	0.1 vol.% Graphene	Water/EG (50:50)	Heat transfer rate (4%) Pressure drops (4.1%)	[33]
Cone helically coiled tube heat exchanger	0.5 vol.% MWCNT (50-80 nm)	Water/EG (70:30)	Nusselt number (52%)	[34]
	0.96 wt.% TiO_2	Water	Heat dissipation capacity (25.6%) Pressure drops (6.1%)	[35]

From the above reviews, most studies suggested that nanoparticles could enhance the heat transfer performance of base coolant or even reduce the size of a radiator, indicating that it could be used as a

substitute for conventional coolant. Various study scopes led to several conclusions on the improved heat transfer performance of using nanocoolant. However, studies on the use of hybrid nanocoolant in an actual vehicle radiator are still limited. Aside from applying nanocoolant in the radiators, there is still no consensus on some mechanisms underlying improved thermal conductivity of nanocomposite.

To the best of the authors' knowledge, few researchers compared hybrid nanocoolants with different mixing ratios. Even though only a few studies have been conducted on the mixing ratio, their findings still have discrepancies. Meanwhile, these studies [22, 36] discovered ascending thermal conductivity with a higher material ratio and good thermal conductance. On the other hand, another group of researchers [37, 38] demonstrated that the thermal conductivity and thermal performance of hybrid nanocoolant do not change orderly with mixing ratio but are somehow related to solid nanoparticles intercalation. Thus, there is no consensus on the effect of the mixing ratio on the thermal behaviour of hybrid nanocoolants.

The current work compared the thermal performance of graphene-based hybrid nanocoolant with different mixing ratios in a test rig designed to simulate a vehicle cooling system. Various nanoparticles concentration, Reynolds numbers, and air velocities were considered. Lastly, correlations based on the mixing ratio were developed, contributing to the best thermal performance under testing conditions. It should be noted that the authors' previous work on the characterisation, preparation technique, stability, and thermophysical properties of the hybrid nanocoolant used in the current work has been reported here [39].

2.0 Methodology

2.1 Information of Nanocoolant

DW/EG were mixed in a 60:40 weightage ratio as a base coolant. The nanoparticles in the base coolant were composed of various TiO_2 ratios and carboxyl-functionalised graphene nanoplatelets (CGnP). For each test, 3 L of nanocoolant was prepared by vigorous stirring for 40 min and ultrasonication for 90 min. The designation of all nanocoolant used in the current study is tabulated in Table 2.

Table 2. Details of all nanocoolant used in the present study

The concentration of nanoparticles (wt.%)	Mixing ratio (CGnP-TiO_2)	Designation
0.1	100:0	0.1 wt.% 10G
	70:30	0.1 wt.% 7G-3T

0.075	50:50	0.1 wt.% 5G-5T
	30:70	0.1 wt.% 3G-7T
	100:0	0.075 wt.% 10G
	70:30	0.075 wt.% 7G-3T
	50:50	0.075 wt.% 5G-5T
	30:70	0.075 wt.% 3G-7T
0.05	100:0	0.05 wt.% 10G
	70:30	0.05 wt.% 7G-3T
	50:50	0.05 wt.% 5G-5T
	30:70	0.05 wt.% 3G-7T
0.025	100:0	0.025 wt.% 10G
	70:30	0.025 wt.% 7G-3T
	50:50	0.025 wt.% 5G-5T
	30:70	0.025 wt.% 3G-7T

2.2 Experimental Setup

Figure 1 and Figure 2 present a photo and a schematic diagram of the heat transfer test rig used in the study, respectively. Stainless steel 304 pipes (internal diameter: 1.5 cm, thickness: 2 mm) were used to prevent corrosion and erosion. A 5 mm thick glass wool was wrapped around the pipes as an insulator to minimise heat loss. For each run, the 5 L tank was filled with 3 L of coolant. A 25 mm thick heat insulator was applied to the band heater to reduce heat loss and ensure safety. Shimaden temperature controller (model: SRS 10A, 250 V, AC, resolution of 0.1 °C) with a sheath thermocouple with a band heater was used to maintain the coolant temperature. An actual vehicle radiator (Perodua Kancil) was used as the heat exchanger, with 31 tubes and 32 columns of serpentine fins. The radiator's geometrical details are labelled and tabulated in Figure 3 and

Table 3, respectively.

An industry fan (Gold Lux, 350 mm, 50 W) was installed to imitate flowing air from the surroundings. The fan was placed 20 cm away from the radiator surface, and the space in between was covered with a 35 x 35 cm^2 cross-sectional area aluminium rectangular airflow duct. A magnet pump (Sanso PMD-221, IP44, maximum operating temperature of 60 °C) with a constant flow rate of 780 L/hour was

installed before a rotameter (New-flow, model: MF200, SS316 material, IP65 protection class, 0 - 150 °C), and the desired flow rate was adjusted using a ball valve.

Two pairs of RTD PT-100 sensors (Maltec-T, 0-150 °C) and pressure transmitter (Huba, 0-6 bar, 125 °C) were used to measure working fluid bulk temperature (average of inlet and outlet temperature) and pressure, respectively. Both RTD-100 sensors were placed 15 cm apart from the radiator's inlet and outlet, and the gap between them was covered entirely with glass wool. All sensors were connected to a paperless recorder (Ohkura, model: VM7000A). Five k-type thermocouples (Maltec-T, 0 - 200 °C) were attached to the radiator surface at different points to measure the radiator tube surface temperature. An anemometer (UT363, 0 - 30 m/s with 0.1 m/s of resolution) was used to measure the temperature and velocity of flowing air.

The coolant flow rate range was selected based on past experimental studies that employed crossflow type radiators [40-44]. Since the present research considered the pump and pipe size limitations, the coolant flow rate was fixed between 100 to 600 L/hour (1.67 to 10 L/min). Three different air velocities (1.7 - 2.1 m/s) were obtained using the cooling fan's default adjustable speeds. At all testing conditions, a room temperature of 27 ± 1 °C was used to cool the radiator.

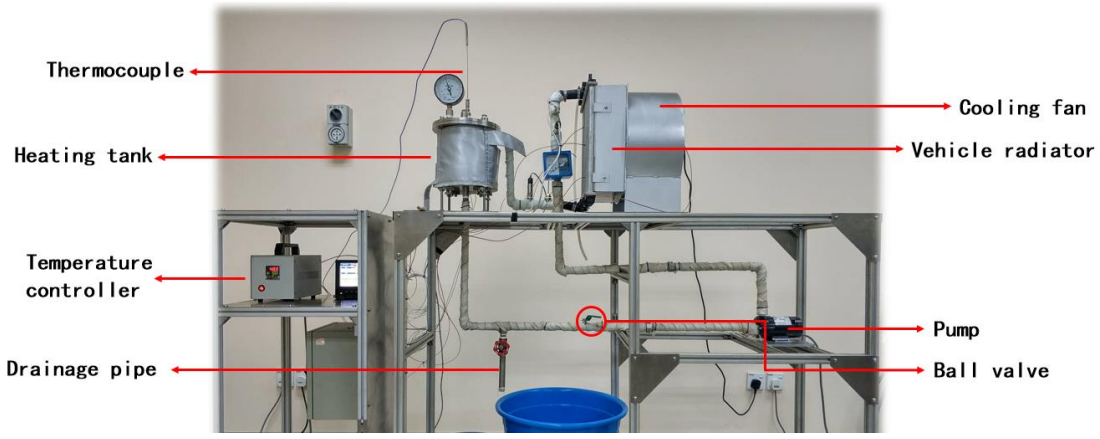

Figure 1. Test rig for obtaining heat transfer performance of the coolant

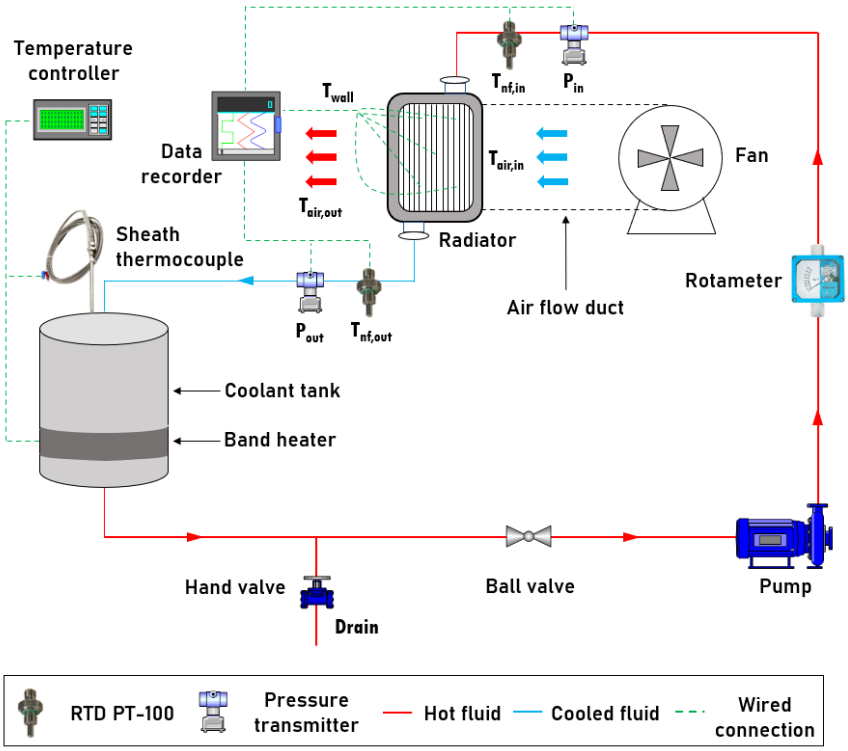

Figure 2. The schematic diagram for the heat transfer test rig

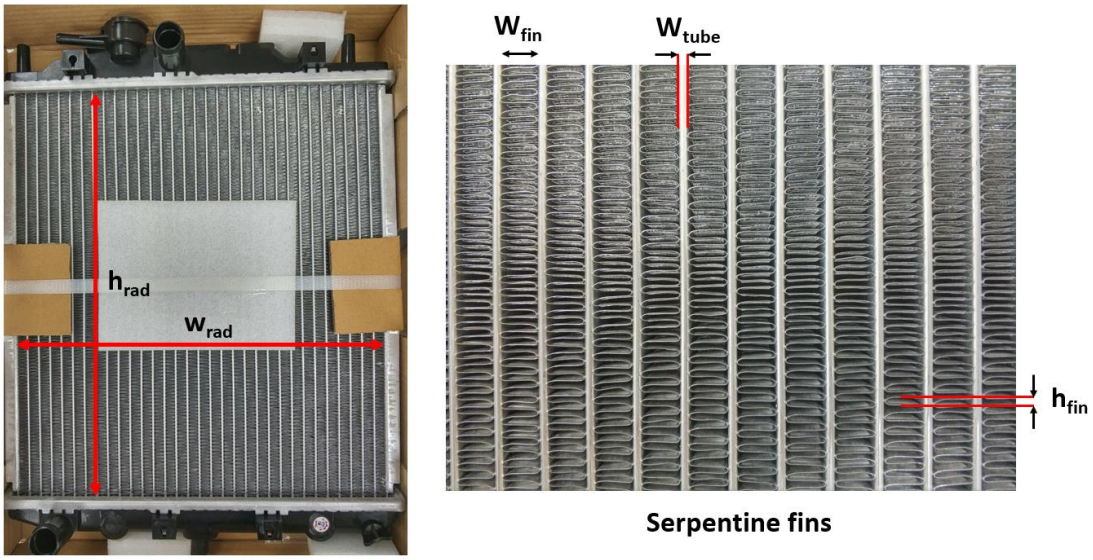

Figure 3. Structure of crossflow radiator and type of fins used in the current study

Table 3. Measured geometrical properties of radiator and fin

Feature	Notation	Configuration
Radiator height	h_{rad}	0.368 m
Radiator length	l_{rad}	0.0165 m

Tube length	l_{tube}	0.0158 m
Tube thickness	t_{tube}	0.002 m
Tube hydraulic diameter	$D_{h,tube}$	0.002181559 m
Number of tubes	n_{tube}	31
The cross-sectional area of each tube	$A_{tube,cross}$	0.0000192344 m^2
The outer surface area of each tube	$A_{tube,outer}$	0.036908867 m^2
Tube and fin material	-	Aluminium
Fin height	h_{fin}	0.0016 m
Fin length	l_{fin}	0.0165 m

2.3 Experimental Procedure

Following the sonication, 3L of nanocoolant was poured into the reservoir tank and heated to 35.0 ^oC using a band heater. The required coolant volume flow rate and fan speed were adjusted and allowed to flow for at least 30 minutes to attain a steady condition (inlet temperature of 35.0 ^oC). The room (ambient) temperature was measured with an anemometer and thermocouple before data acquisition. Following that, data was continuously recorded for 10 minutes. The whole process was repeated at least twice to ensure that the results were repeatable. The recorded readings were used to compute the essential parameters listed in Section 2.5.

For data verification purposes, heat balance error was first computed in the test rig using base coolant. After obtaining an acceptable range of results, the Nusselt number obtained was compared to the well-known Dittus-Boelter equation and four common laminar correlations, namely Maiga et al. [45], Dehghandokht et al. [46], Shah-London [47] and Sieder-Tate al. [48]. Finally, the radiator's overall heat transfer coefficient and effectiveness were compared, followed by Minitab software correlations.

2.4 Assumptions

Along with the test rig, the nanocoolant's temperature varied due to heating at the reservoir tank and cooling at the radiator. Consequently, the thermophysical properties of the nanocoolant, which were significantly affected by temperature change, had an impact on the computation of various performance parameters. Few assumptions commonly used by past researchers have been implemented in this research to simplify calculations with minor inaccuracy significantly:

1. No or negligible heat loss to the surrounding. Due to the insulated pipe outer surface, the temperature difference between the flowing coolant and the pipe wall surface is considered insignificant. The test rig is also allowed to operate for 30 min to achieve a steady state.

Furthermore, the gap between RTD PT-100 sensors and the radiator's inlet/outlet is fully insulated. In this way, bulk temperature (T_b) can be considered as average fluid temperature.

2. Steady fluid flow. Flow rate and coolant velocity are assumed to be constant when operating conditions are constant for an extended period. Besides, the high stability or homogeneity of nanocoolant implies constant density and viscosity at all points. A fully covered air duct also helps to reduce turbulence and temperature changes caused by the surrounding flowing air.

3. Due to minimal radiator tube thickness (t ≈ 0.0002 m), it is assumed that no heat resistance exists between the outer and inner wall temperature.

2.5 Data Reduction

Bulk temperature, T_b can be computed using Equation (1).

$$T_{b,nc} = \frac{T_{nc,in} + T_{nc,out}}{2} \tag{1}$$

Based on Equation (1), subscripts nc, in, and out are nanocoolant, inlet, and outlet, respectively.

Heat transfer occurs at the test rig when the flowing air cools the hot coolant through the radiator surface. The heat transfer rate from both the cooling and heating processes is as follows:

$$\dot{Q}_{tube} = \dot{m}_{nc}(C_p)_{nc}(T_{nc,in} - T_{nc,out}) \tag{2}$$

$$\dot{Q}_{air} = \dot{m}_{air}(C_p)_{air}(T_{air,out} - T_{air,in}) \tag{3}$$

Where $\dot{Q}$ is the heat transfer rate, $\dot{m}$ is the mass flow rate, C_p is the specific heat capacity, and the subscript tube and air represent the tube side (cooling) and airside (heating), respectively. However, the heat transfer rates from both sides would not be equal due to various factors such as heat loss, experimental error, and environmental effects. Thus, an error caused by heat loss can be determined using heat balance relative error (e_{hb}) [49]:

$$e_{hb} = \frac{\dot{Q}_{tube} - \dot{Q}_{air}}{\dot{Q}_{ave}} \times 100 \quad (4)$$

$$\dot{Q}_{ave} = \frac{\dot{Q}_{tube} + \dot{Q}_{air}}{2} \quad (5)$$

Based on Equations (4) and (5), $\dot{Q}_{ave}$ is the average heat transfer rate and will be applied when the deviation between both sides is slight.

Since the heat transfer process at the radiator tube side involves both a fluid and a solid surface, the convection heat transfer coefficient (h_{in}) is computed using Equation (6).

$$\dot{Q}_{tube} = h_{in} A_{tube,inner} \left(T_b - T_{wall} \right) \quad (6)$$

Where h_{in} is the internal heat transfer coefficient inside the tube, $A_{tube,\ inner}$ is the inner surface area of the tube, and T_{wall} is the average wall temperature of different points across the radiator tube surface.

$$T_{wall} = \frac{T_1 + T_2 + T_3 + T_4 + T_5}{5} \quad (7)$$

When analysing a radiator, combining all thermal resistances is preferable and computing an overall heat transfer coefficient (U). The U is related to Newton's law of cooling as follows:

$$U = \frac{\dot{Q}_{ave}}{A_s \Delta T_{LMTD}} \quad (8)$$

Whereby A_s is the heat transfer surface area and ΔT_{LMTD} is the log mean temperature difference (LMTD). It should be noted that the U of the radiator can be specified on either the tube side or air side by changing its specific heat transfer area. LMTD represents the average temperature difference between both coolant and air in the hot and cold states. However, ordinary LMTD is not accurate for crossflow-type heat exchangers, and hence a correction factor, F, is applied for the deviation.

$$\Delta T_{LMTD} = F \Delta T_{LMTD,CF} \tag{9}$$

$$\Delta T_{LMTD,CF} = \frac{(T_{nc,in} - T_{air,out}) - (T_{nc,out} - T_{air,in})}{\ln(\frac{T_{nc,in} - T_{air,out}}{T_{nc,out} - T_{air,in}})} \tag{10}$$

Based on Equations (9) and (10), subscript CF stands for crossflow-type heat exchanger. The F can be obtained from correction factor charts or defined as shown in Equations (11 - 13):

$$F = \frac{\ln[(1-RS)/(1-S)]}{(1-1/R)\ln[1+R\ln(1-S)]} \tag{11}$$

$$R = \frac{(T_{air,out} - T_{air,in})}{(T_{nc,in} - T_{nc,out})} \tag{12}$$

$$S = \frac{(T_{nc,out} - T_{nc,in})}{(T_{air,in} - T_{nc,in})} \tag{13}$$

Another non-LMTD approach was used for computing the U in many studies. The U_{air} obtained using Equations (8) and (14) was compared in the present study.

$$U_{air} = \frac{1}{\frac{1}{\eta_o h_{air}} + \frac{1}{(\frac{A_{in}}{A_{air}})h_{in}}} \tag{14}$$

Where η_o is the finned surface efficiency, h_{air} is an airside convective heat transfer coefficient, and A is the heat transfer area. Subscripts in and air represent the airside and tube side, respectively.

Next, one of the most common dimensionless parameters representing heat transfer enhancement is the Nusselt number, the ratio of convective heat transfer overheat transfer through conduction. The Nusselt number is defined as:

$$Nu = \frac{h_{in} D_h}{k_b} \tag{15}$$

Where Nu is the Nusselt Number, k_b is the thermal conductivity of coolant at bulk temperature, and D_h is the hydraulic diameter of the pipe. The Nusselt number calculated using Equation (15) was compared to the Nusselt number computed using correlations to verify the experimental results obtained. These equations can be used to compute the Nusselt number for both base coolant and nanocoolant.

Meanwhile, the widely used Dittus-Boelter equation defines the Nusselt number as:

$$Nu = 0.023\, Re^{0.8} Pr^{0.4} \tag{16}$$

Where Re and Pr are computed based on the bulk temperature of the coolant. Many researchers compared their experimental results using the Dittus-Boelter equation. Although this equation is best suited to internal turbulent flow in a single tube, it is widely employed in heat exchanger applications. For data verification, some laminar flow correlations that are reliable in numerous studies were chosen. Nusselt number from the correlations can be expressed as Equations (17), (18), and (19).

Maiga et al. [45]:

$$Nu = 0.951\, Re^{0.173} Pr^{\frac{1}{3}} \tag{17}$$

Dehghandokht et al. [46] for compact heat exchanger:

$$Nu = 0.28\, Re^{0.35} Pr^{0.36} \tag{18}$$

Sieder-Tate [50]:

$$Nu = 1.86(\mathrm{Re}\cdot \mathrm{Pr})^{\frac{1}{3}} \left(\frac{D_h}{l_{fin}}\right)^{\frac{1}{3}} \left(\frac{\mu_b}{\mu_s}\right)^{0.14} \tag{19}$$

Where l is the length of the fin, μ is the fluid viscosity at the bulk fluid temperature, and μ_s is the fluid viscosity at the heat-transfer boundary surface temperature.

Shah and London [47] for Reynolds number > 33.33:

$$Nu = 1.953(\mathrm{Re}\cdot \mathrm{Pr}\frac{D_h}{l_{fin}})^{\frac{1}{3}} \tag{20}$$

Reynolds number is defined as the ratio of inertia force to viscous force.

$$Re = \frac{\rho_b v_b D_h}{\mu_b} \tag{21}$$

Re is Reynolds Number, ρ is density, v is velocity, and μ is dynamic viscosity. All three properties were taken at the bulk temperature of the coolant.

The Prandtl number is the ratio of momentum diffusivity to heat diffusivity. A high value indicates that the substance's velocity boundary layer is thicker than its thermal boundary layer and vice versa.

$$\mathrm{Pr} = \frac{\mu_b (C_p)_b}{k_b} \tag{22}$$

Based on Equation 22, Pr is Prandtl number, *Cp* and *k* are specific heat capacity and thermal conductivity of coolant at bulk temperature, respectively.

Meanwhile, the effectiveness of crossflow type heat exchanger can be expressed as:

$$\varepsilon = 1 - \exp\{\frac{NTU^{0.22}}{c}[\exp(-c\cdot NTU^{0.78}) - 1]\} \tag{23}$$

$$NTU = \frac{UA_s}{C_{\min}} = \frac{UA_s}{(\dot{m}C_p)_{\min}} \tag{24}$$

$$c = \frac{C_{\min}}{C_{\max}} \tag{25}$$

whereby NTU is the number of transfer units, c is the capacity ratio, C is the heat capacity rate, U is the overall heat transfer coefficient, A_s is the heat transfer area, $\dot{m}$ is the mass flow rate, and c_p is the specific heat capacity. The subscripts min and max are minimum and maximum, respectively.

2.6 Uncertainty Analysis

Experiment work entails a significant amount of measurement with various sensors and equipment. Uncertainty in performance parameters is dependent mainly on the accuracy of the instrument used. The method to estimate uncertainty was suggested by Moffat [51], as shown in Equation (26).

$$u_R = [(\frac{\partial R}{\partial x_1} u_1)^2 + (\frac{\partial R}{\partial x_2} u_2)^2 + \cdots + (\frac{\partial R}{\partial x_n} u_n)^2]^{\frac{1}{2}} \quad (26)$$

Dependent variable (R) is defined as a function of independent variables x_1, x_2, …, x_n; hence $R = R$ (x_1, x_2, …, x_n). While u_R is the uncertainty of the dependent variable and u_1, u_2 …, u_n is the uncertainties of independent variables. The uncertainties for performance parameters in the present work are tabulated in Table . Meanwhile, the equipment and apparatus were obtained from the suppliers.

Table 4. Accuracy of instruments and uncertainty of performance parameters

Equipment/Parameter	Accuracy	Uncertainty
Weighing balance	± 5%	-
Type-k thermocouple	± 0.5%	-
RTD Pt-100	± 0.067%	-
Flowmeter	± 2%	-
Anemometer	± 3.334 % (Temperature) ± 5 % (Wind speed)	-
Nanoparticle concentration	-	± 5%
Reynolds number	-	± 2%
Tube side heat transfer rate	-	± 2%
Airside heat transfer rate	-	± 6.01%
Convective heat transfer coefficient	-	± 2.06%
Nusselt number	-	± 2.06%
Overall heat transfer coefficient	-	± 3.89%

3.0 Results and Discussions

3.1 Verification of Experimental Data

The heat transfer rates for both the cooling and heating sides were estimated using Equations (2) and (3), respectively, before being compared. For verification, the inlet temperature and air velocity (v_{air}) were fixed at 35 ºC and 1.7 m/s, respectively. For Reynolds number of 46, 111, 176, 241, 305, and 369, the errors of heat balance (e_{hb}) shown in Figure 4 are 11.5%, 8.38%, 7.57%, 9,59%, 10.7%, and 8.26%, respectively. ASME PTC 30-1991 states that a maximum error of less than ± 15% is acceptable. Therefore, the average heat transfer rate ($\dot{Q}_{ave}$) is appropriate for calculating the overall heat transfer coefficient (Equation 8), as this calculation was applied in previous studies [9, 52]. The differences in heat transfer rate are most likely due to heat loss from the radiator and the fluctuations in room air temperature during the operation of the experiment.

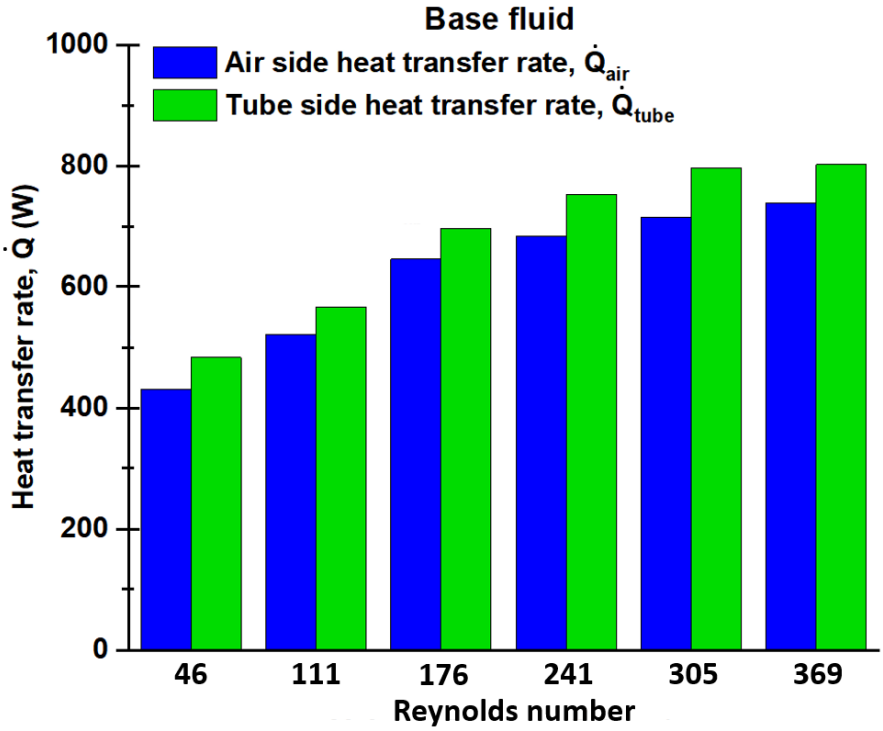

Figure 4. Verification of experimental data by judging heat balance error at different Reynolds numbers.

Next, the Nusselt number was computed using correlations and compared to recorded data, as shown in Figure 5. The testing conditions were the same as for the heat balance error verification. The experimental data was found to be in good agreement with Dehghandokht and Shah-London's

correlation. The deviation of the experimental Nusselt number is tabulated in **Error! Reference source not found.**.

Table 5. Deviation of experimental Nusselt number (base coolant) from correlations

Correlation	Average deviation	Mean absolute deviation (MAD)	Standard deviation
Dehghandokht et al. [46]	6.163%	0.7752	0.995
Shah-London [47]	12.65%	0.7932	1.019

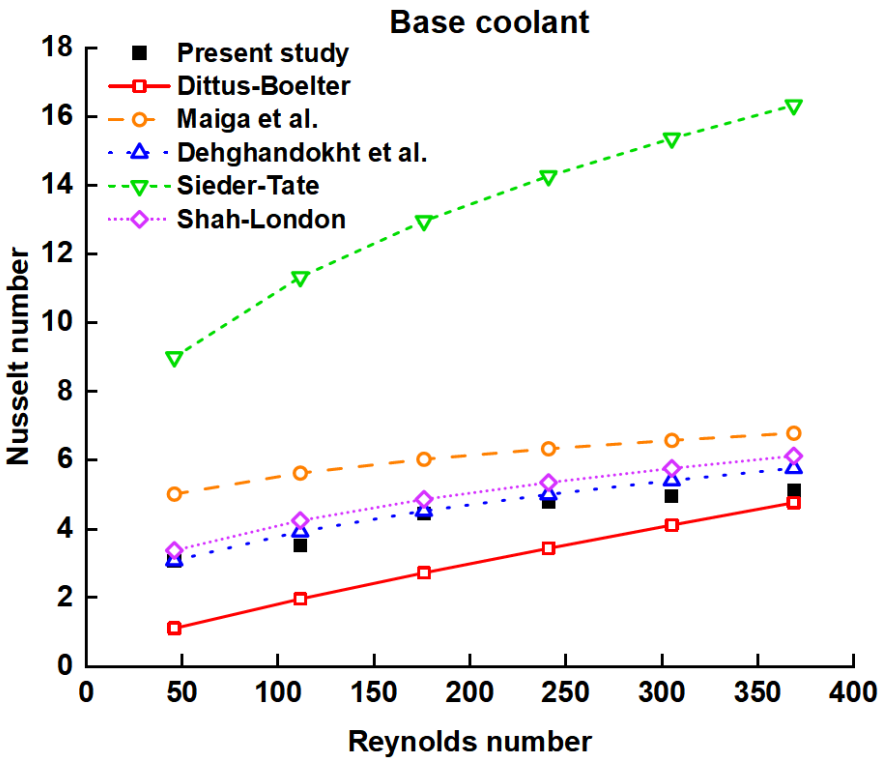

Figure 5. Nusselt number of base coolants obtained from experiment and computed using different correlations at an air velocity of 1.7 m/s.

3.2 Pressure Drop

A pressure drop increment of 4 kPa to 8 kPa was recorded for all nanocoolant (including base coolant) when the coolant flow rate was increased from 100 to 600 L/hour under all testing conditions. However, adding nanoparticles to the base coolant did not result in discrepancies due to the pressure transmitter's limitation (non-readable for pressure < 999 Pa). Hence, the pressure drop results are not reported. Previous studies showed that the addition of nanoparticles increased pressure drop by 1 to 4% [20, 24, 53] and increased heat transfer by more than 10%. These findings resulted in optimal performance of the factor, and thus judging heat transfer performance in this study was feasible.

3.3 Heat Transfer Performance

3.3.1 Nusselt Number

Figure 6 shows the effect of nanoparticle concentration and Reynolds number on Nusselt number at different air velocities. A higher concentration of nanoparticles resulted in greater heat transfer since more solid particles can remove heat during the cooling process. The lowest concentration (0.025 wt.%) of 10G nanocoolant showed heat transfer deterioration at all air velocities due to its low thermal conductivity [39]. At low Reynolds number (50) and air velocity of 1.7 m/s, Nusselt number of base coolants was slightly increased by 3.02%, 3.11%, 3.15% and 3.16%, when 0.025 wt.%, 0.05 wt.%, 0.075 wt.%, and 0.1 wt.% of CGnP was added. When the air velocity was increased to 1.9 and 2.1 m/s, 0.1 wt.% 10G at the same Reynolds number improved by 10.8% and 19.2%, respectively. A similar enhancement was also observed for 5G-5T nanocoolant due to comparable thermal conductivity value.

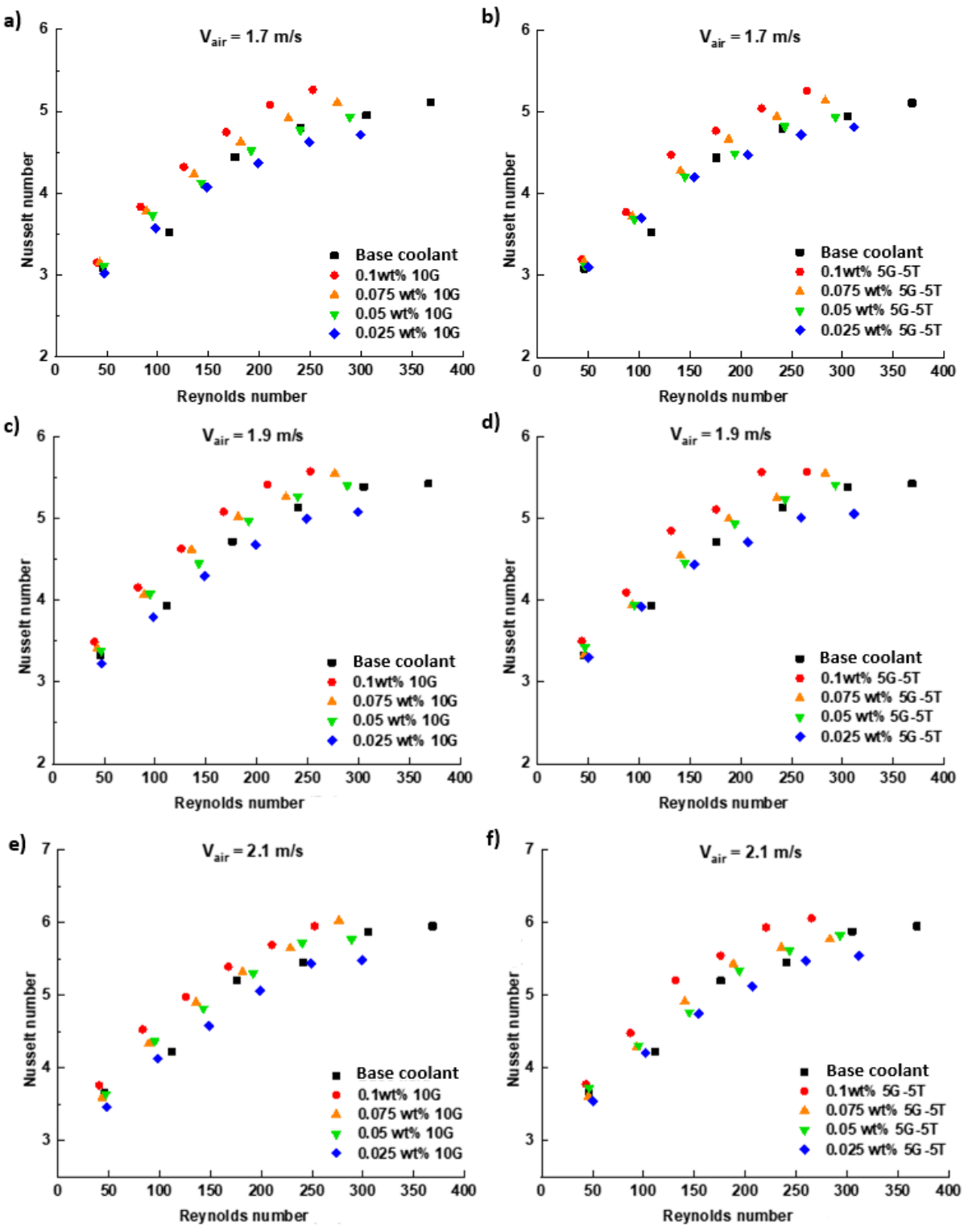

Figure 6. Effect of nanoparticles concentration on Nusselt number on 10G and 5G-5T nanocoolant. a), b) 1.7 m/s; c), d) 1.9 m/s; e), f) 2.1 m/s

Based on Figure 7, the mixing ratio has the same effect on the Nusselt number as it does on thermal conductivity. As expected, the Nusselt number of 7G-3T nanocoolant showed the highest Nusselt

number at all testing conditions since 70:30 of mixing ratio exhibits the highest thermal conductivity. The highest Nusselt number (6.19) was obtained at an air velocity of 2.1 m/s and a coolant flow rate of 600 L/hour (Reynolds number = 259) using 0.1 wt.% 7G-3T nanocoolant. On the other hand (refer to Figure 7a and b), at Reynolds number of 50 and air velocity of 1.7 m/s, the lowest Nusselt number obtained was 3.03 from 0.025 wt.% 10G, which was 1.88% lower than the base coolant. At the same air velocity (when Reynolds number was increased to around 300), 0.025 wt.% nanocoolant with mixing ratios of 10G, 7G-3T, 5G-5T, 3G-7T, and base coolant showed Nusselt number of 4.71, 5.16, 4.82, 4.98, and 4.95, respectively. At 0.025 wt.% of concentration, 3G-7T nanocoolant had a similar Nusselt number to the base coolant, whereas 10G and 5G-5T nanocoolant had a lower Nusselt number than the base coolant at all air velocity. Comparing the graphs in Figure 7 by side-to-side (a to b, c to d, e to f), further increases in nanoparticles concentration up to 0.05 wt.% showed little enhancement than the base coolant at all Reynolds numbers. This phenomenon was in line with the thermal conductivity findings. At 600 L/hour of coolant flow rate, both 0.1 wt.% 10G (Reynolds number = 252) and 0.1 wt.% 5G-5T (Reynolds number = 265) showed similar Nusselt numbers at 1.7 m/s and 1.9 m/s of air velocity. When it came to 2.1 m/s, 0.1 wt.% 5G-5T had a 1.81% higher Nusselt number than 0.1 wt.% mono-nanocoolant.

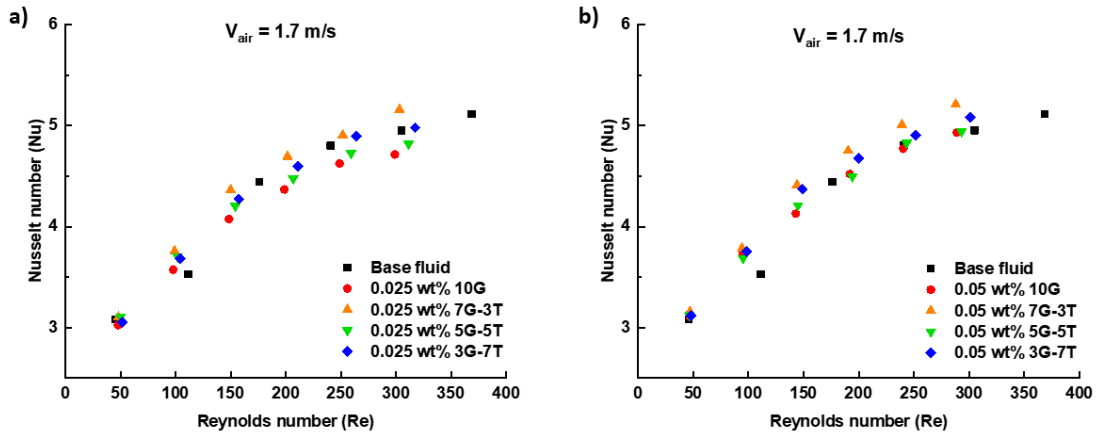

Figure 7. Effect of hybrid mixing ratio on Nusselt number of 0.025 wt.% and 0.05 wt.% nanocoolant. a), b) 1.7 m/s; c), d) 1.9 m/s; e), f) 2.1 m/s

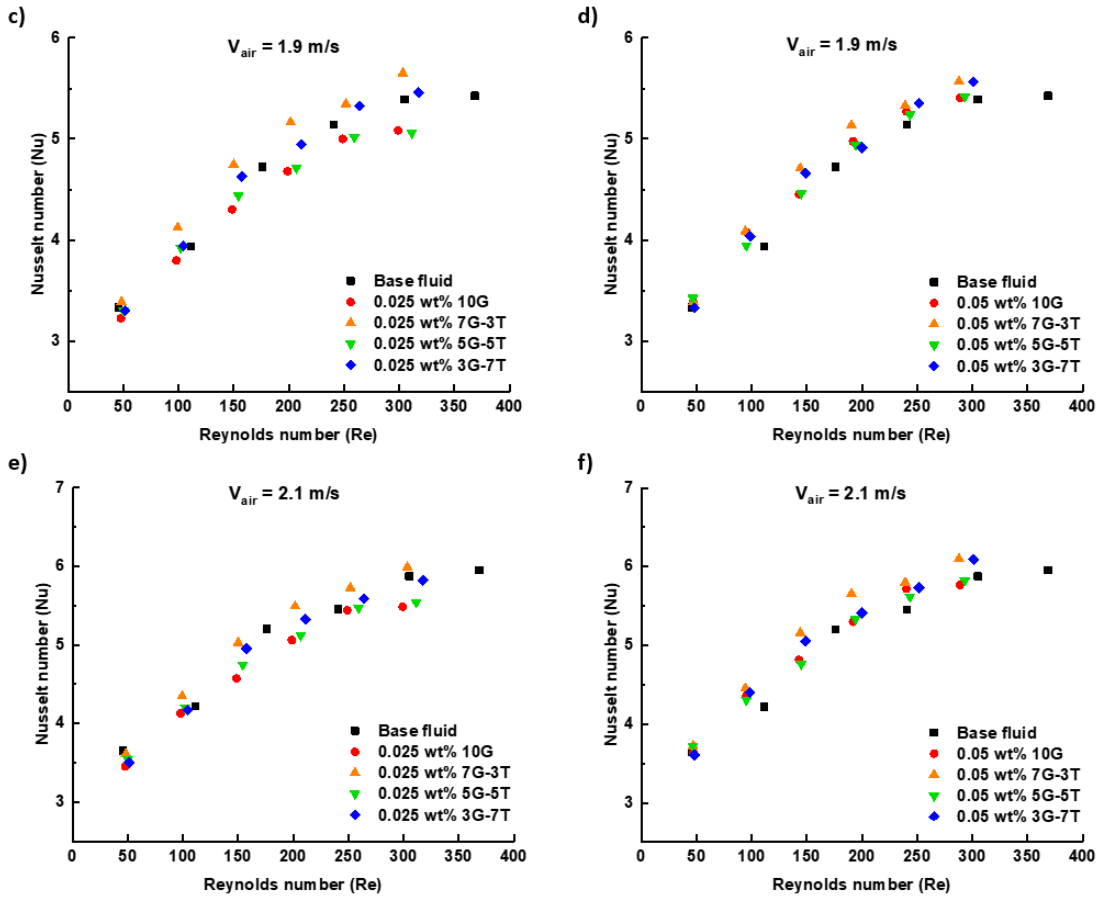

Figure 7. Continued

3.3.2 Overall Heat Transfer Coefficient (OHTC)

In this work, the OHTC was computed based on two different heat transfer areas: air and tube sides. Tube side heat transfer area is the total tubes internal surface area, while the airside heat transfer area is the total external surface area of fins and tubes. As observed in Figure 8, the OHTC of the base coolant for both the airside and the tube side has the same increment due to the calculation adopting the average heat transfer rate ($\dot{Q}_{ave}$). Airside OHTC (U_{out}) exhibited a much lower value than tube side (U_{in}) due to significant differences in the heat transfer area. At the same time, this has proven that adding fins to the tube wall significantly increases the radiator heat transfer area. Since both OHTC obtained the same amount of base coolant increment, remaining discussions focus on only one side of OHTC.

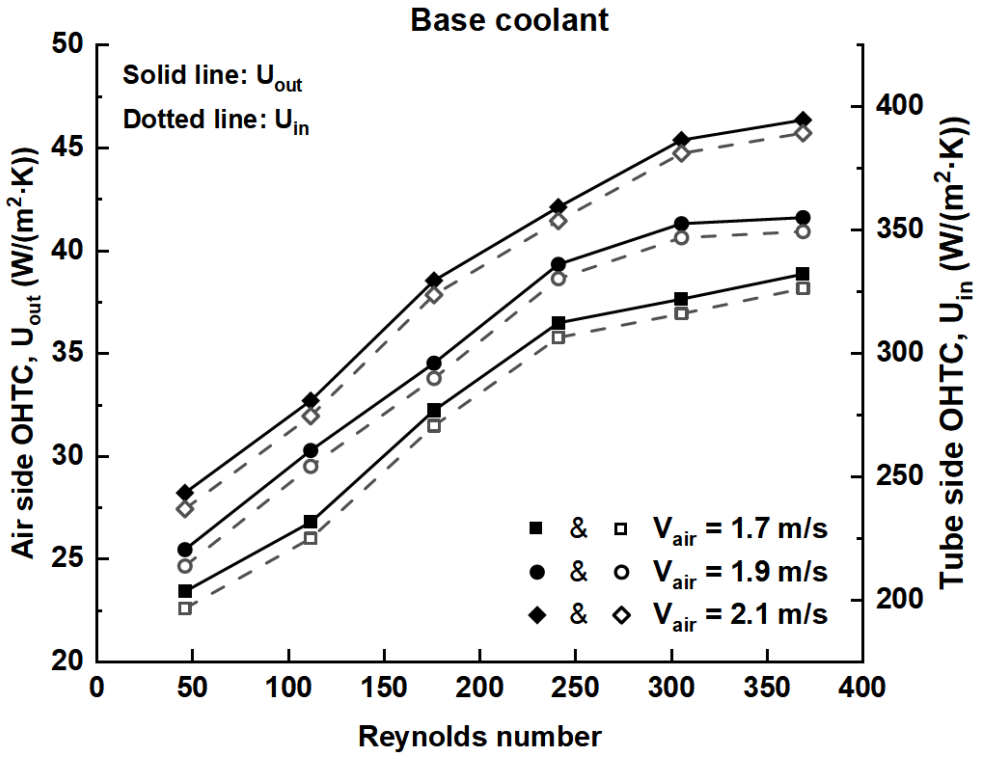

Figure 8. Airside and tube side OHTC of base coolant at different air velocities.

Figure 10 shows how tube side OHTC varies with different concentrations of 10G nanocoolant. The OHTC increased with nanoparticles concentration and the Reynolds number. Same as the Nusselt number, 0.025 wt.% 10G nanocoolant performed slightly worse or similar to the base coolant. At 1.7 m/s air velocity, base coolant with 0.025 wt.%, 0.05 wt.%, 0.075 wt.%, and 0.1 wt.% pure CGnP exhibited OHTC enhancement of 4.73%, 9.14%, 16.1%, and 20.3%, respectively. Even with increased air velocity up to 2.1 m/s, similar enhancement and deterioration were observed for all concentrations. The impact of air velocity was not as significant as that of other variables.

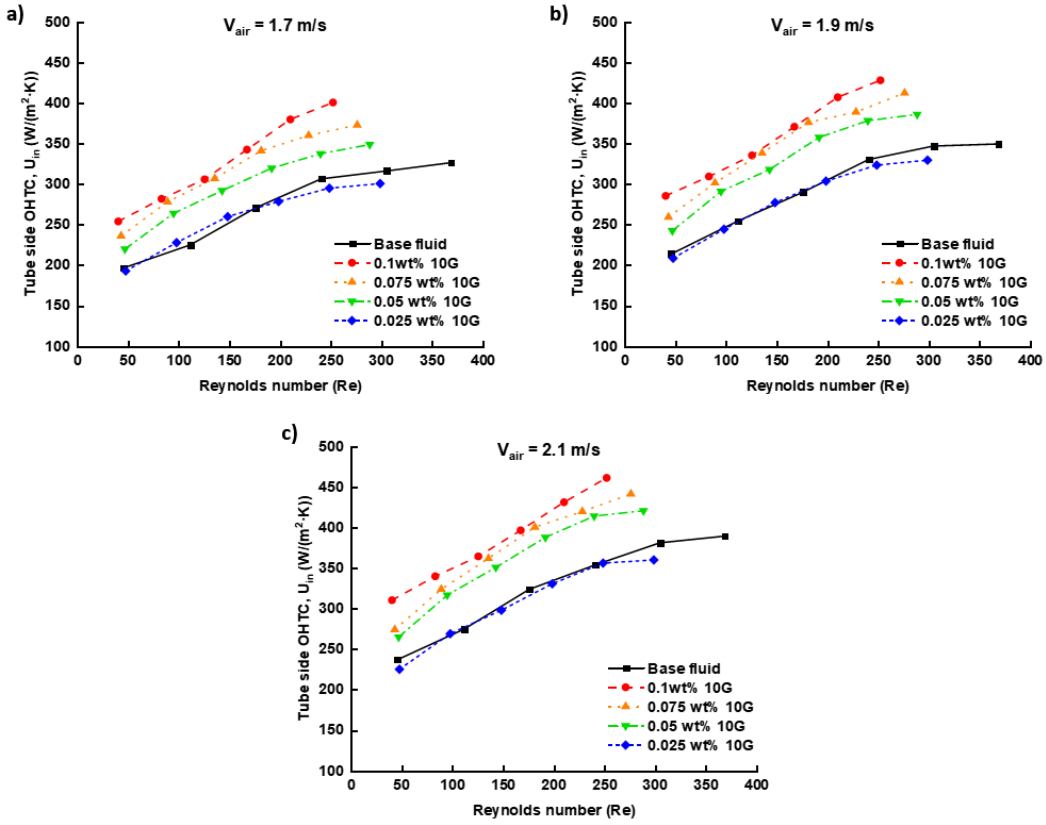

Figure 9. Effect of nanoparticles concentration on tube side OHTC of 10G nanocoolant at different air velocities. a) 1.7 m/s; b) 1.9 m/s; c) 2.1 m/s

At Reynolds number of around 50 and an air velocity of 1.7 m/s, 10G, 7G-3T, 5G-5T, and 3G-7T with 0.075 wt.% of nanoparticles concentration showed higher tube side OHTC of 20.0%, 29.0%, 25.1%, and 28.7%, respectively than base coolant (illustrated in Figure 10a). Other graphs with a slightly fluctuating trend (Figure 10b to 9f) were mostly caused by the average heat transfer rate ($\dot{Q}_{ave}$). Based on Figure 4, the heat balance error between the tube and air sides was not equal for all samples at different Reynolds numbers. The average value may slightly underestimate or overestimate the OHTC of specific samples. Figure 10 (b, d, f) show that for 0.1 wt.% nanocoolant, the average augmentation of tube side OHTC were 16.1%, 28.9%, 23.1%, and 27.8% at 1.7 m/s; 16.7%, 28.0%, 21.6%, and 26.0% at 1.9 m/s; and 13.7%, 26.2%, 19.7%, and 25.1% at 2.1 m/s, using mixing ratio of 100:0, 70:30, 50:50, and 30:70 of CGnP-TiO_2. The mixing ratio of 7G-3T showed the highest OHTC under all operating conditions, like the Nusselt number results. At a coolant flow rate of 600 L/hour, the 7G-3T nanocoolant showed a maximum OHTC enhancement of 34.1% when the nanoparticles concentration was increased from 0% to 0.1 wt.%.

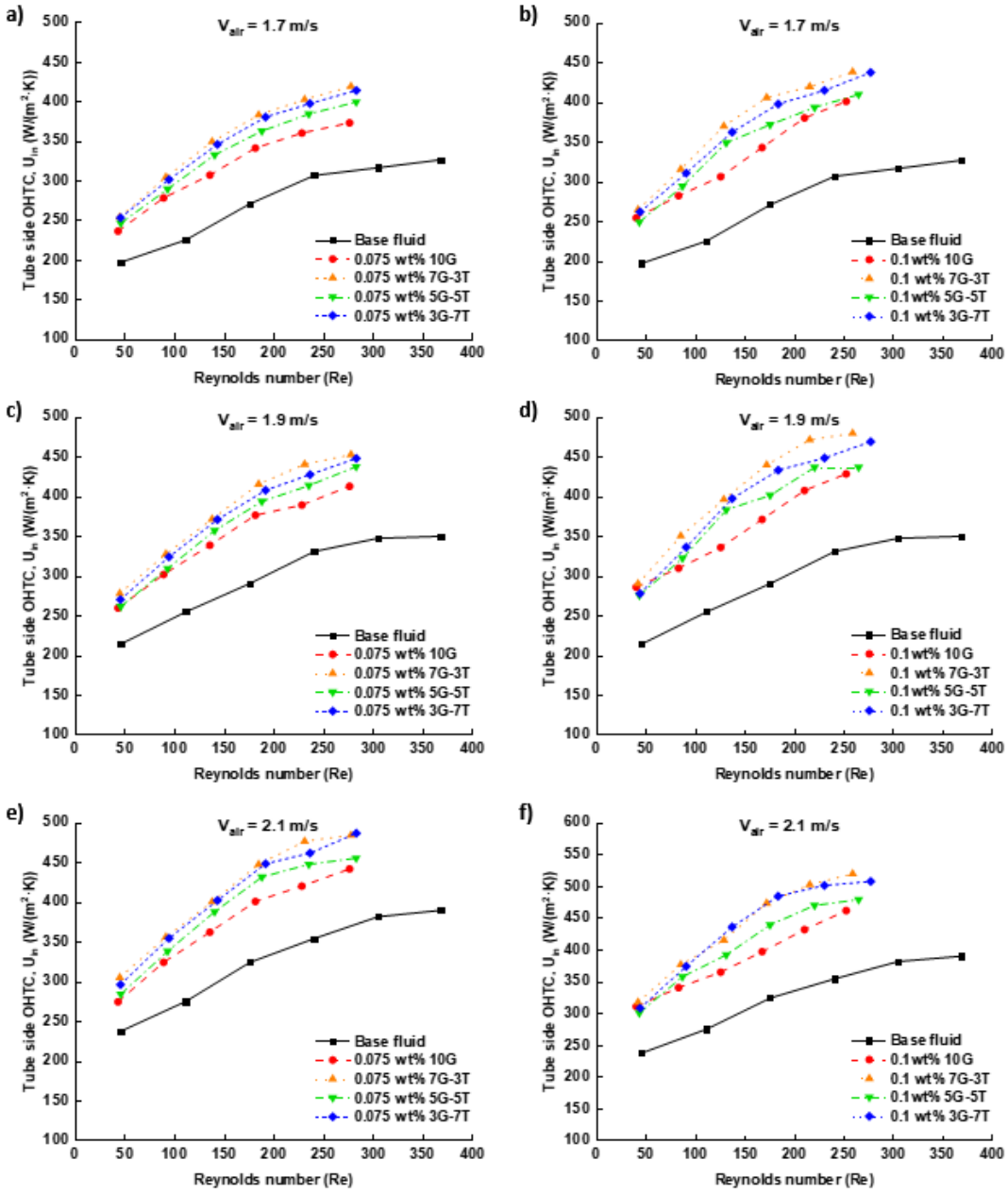

Figure 10. Effect of mixing ratio on tube side OHTC. a), c), e) 0.075 wt.% b), d), f) 0.1 wt.%

Although many studies reported on the thermal performance of nanocoolants in radiators, comparing data with a different set of parameters would not have a significant difference, since the coolant inlet temperature (T_{in} = 35 ^{o}C) and configuration of crossflow type radiator used were the same, only the work of Selvam et al. [54] was compared to the present study. Their nanocoolant was produced by mixing graphene nanoplatelets (GnP) and 70:30 W/EG. Meanwhile, the airside OHTC in their work was computed as in Equation (14).

Figure 11 shows the difference in airside OHTC between the work of Selvam et al. [54] and the present study. Their OHTC increment trend is similar to OHTC from 0.1 wt.% 10G and 0.1 wt.% 7G-3T nanocoolant in the present study. Not only is the coolant inlet temperature similar, but so is the range of air velocity used. This finding acknowledged the wide range of OHTC obtained from the LMTD method in current work. In addition, previous research showed only a slight difference in the OHTC obtained using either the LMTD or the NTU method [52].

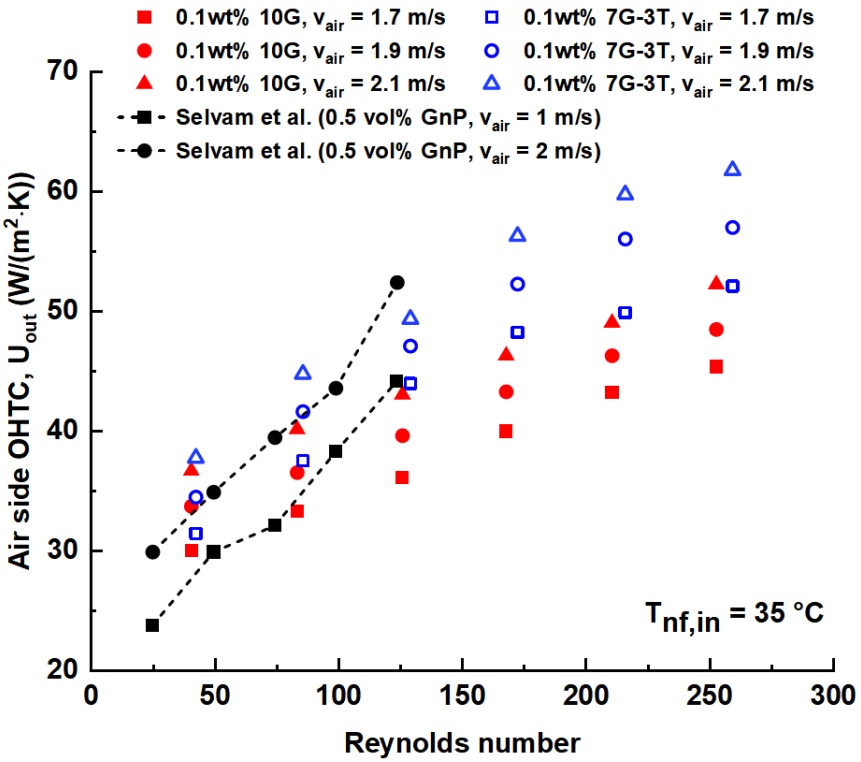

Figure 11. Comparison of airside OHTC with the past study

3.3.3 Effectiveness of Radiator

The effectiveness of the radiator using a base coolant and a nanocoolant is compared in Figure 12. At 1.7 m/s (Reynolds number of 50), adding 0.025 wt.%, 0.05 wt.%, 0.075 wt.%, and 0.1 wt.% of CGnP-TiO_2 (70:30) into base coolant enhanced the effectiveness of radiator by 7.93%, 13.5%, 15.8%, and 18.9%, respectively. When the air velocity was increased to 2.1 m/s at the same Reynolds number, the enhancement was 6.74%, 13.1%, 6.16%, and 16.9% by adding nanoparticles (70:30 CGnP-TiO_2) from

the lowest concentration to the highest. This pattern showed the improvement in heat transfer caused by the addition of nanoparticles.

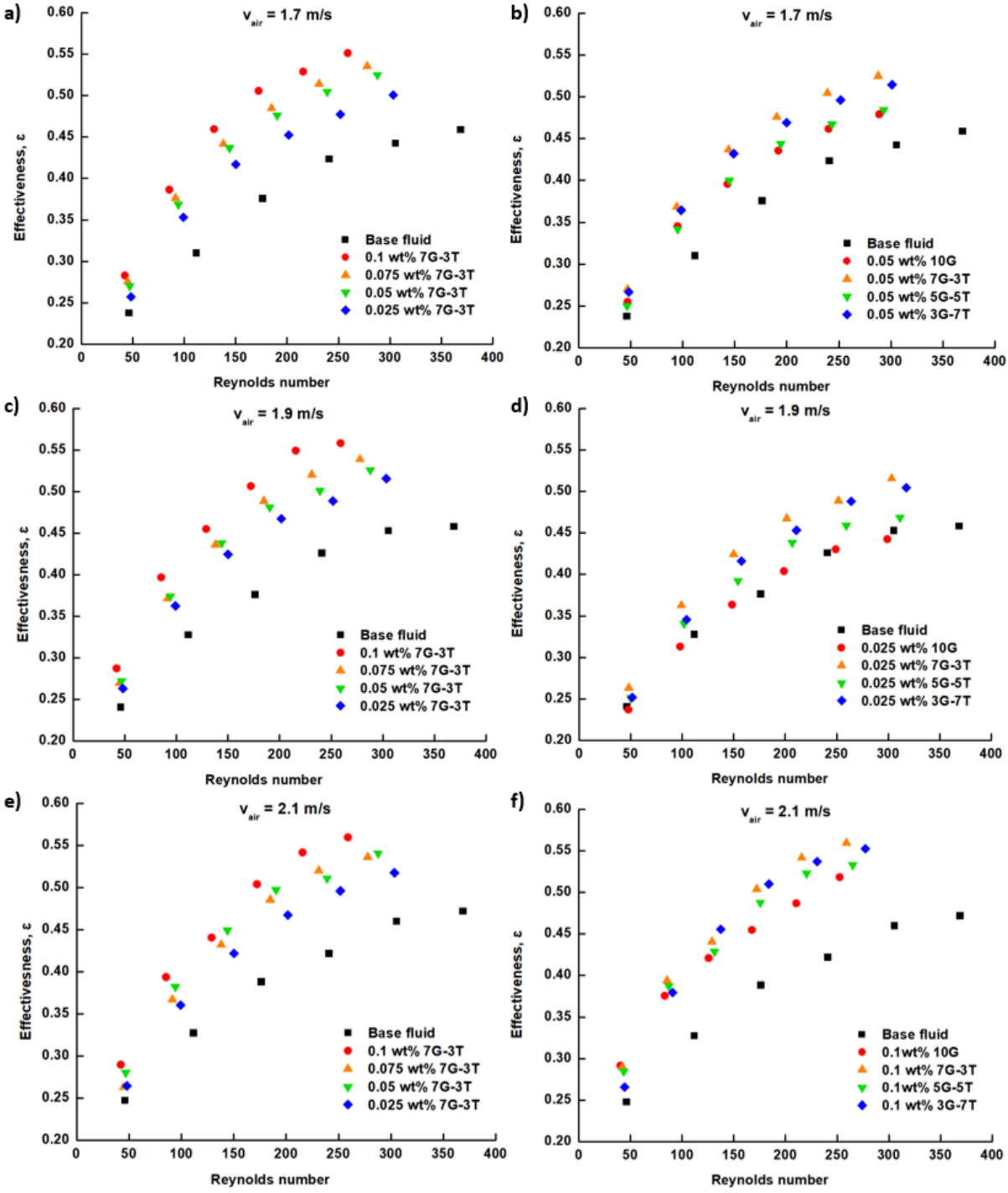

Figure 12. Different effects on the effectiveness of radiator. a), c), e) Nanoparticle's concentration; b), d), f) Mixing ratio

However, the effect of air velocity showed minimal effect on the radiator's effectiveness. At a Reynolds number of 368, the effectiveness of the base coolant was 0.46, 0.46, and 0.47 at 1.7, 1.9, and 2.1 m/s air velocity, respectively. The addition of nanoparticles to the base coolant had a negligible effect on effectiveness, as shown in Figure 13. When air velocity was increased from 1.7 m/s to 1.9 m/s and 2.1 m/s, 0.025 wt.% 7G-3T (Reynolds number = 303) increased by 2.98% and 3.34%; 0.05 wt.% 10G (Reynolds number = 288) enhanced by 2.39% and 2.97%; and 0.075 wt.% 3G-7T (Reynolds number = 283) improved by 0.34% and 1.10%. The low gap of air velocity used (+ 0.2 m/s) and the small temperature difference between cooling air (27 ^{o}C) and coolant inlet temperature (35 ^{o}C) may explain the limited increment observed from air velocity, subsequently affect the heat transfer. Based on Equation (23), a high value of heat capacity rate (C_{min}) caused by an increase in air velocity reduces NTU value even though the average heat transfer rate ($\dot{Q}_{ave}$) increases with air velocity. As a result, the air velocity effect produced a smaller increment in the effectiveness than the Nusselt number and OHTC. Coolant volume flow rate and nanoparticle concentration have a greater influence than inlet air velocity. The same trend has been observed in past studies with other working factors [8, 21, 53].

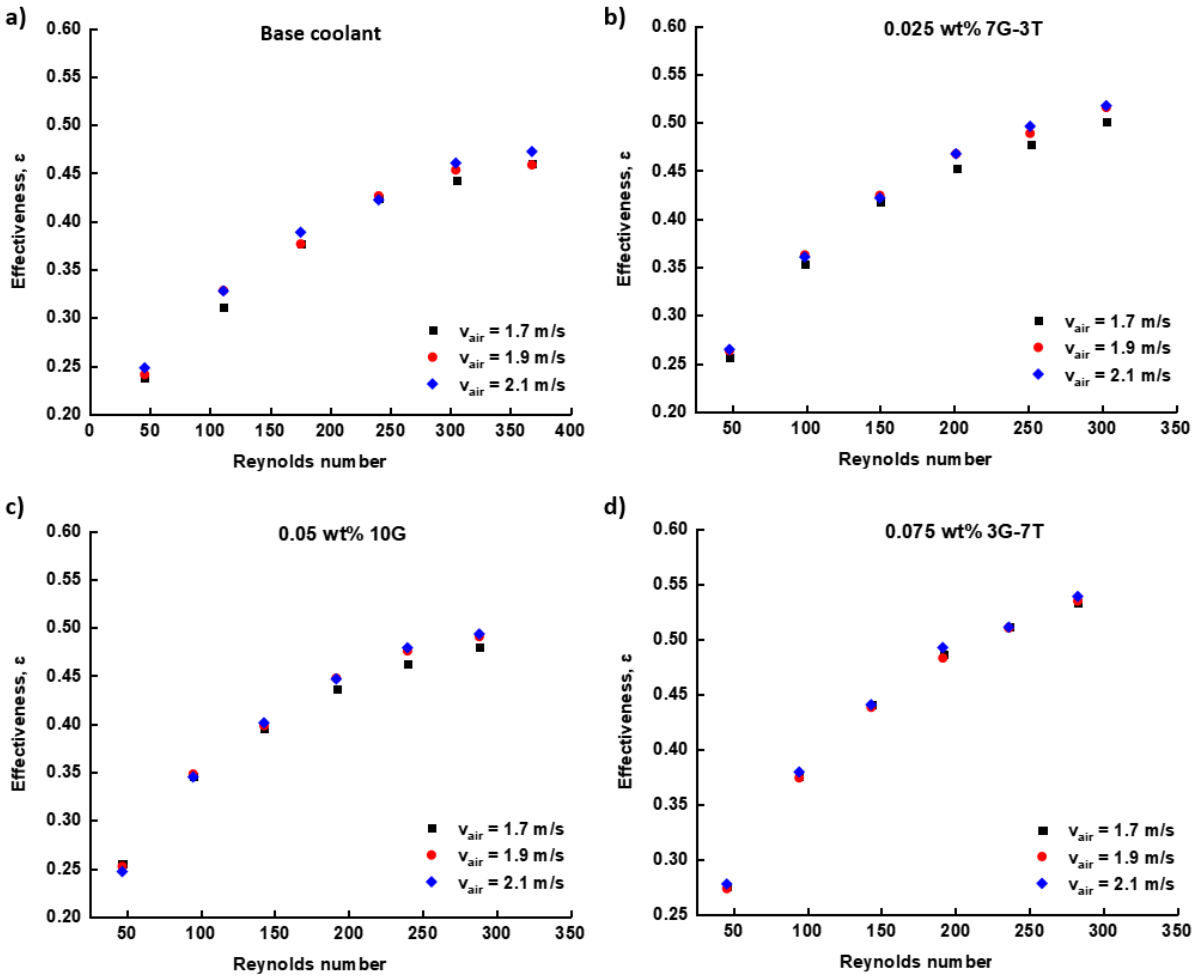

Figure 13. Effect of air velocity on the effectiveness of radiator

The highest effectiveness was achieved within the range of study by using a mixing ratio of 7G-3T (0.56), followed by 3G-7T (0.55), 5G-5T (0.53), 10G (0.52) at the highest nanoparticles concentration and finally, base coolant (0.47). All the earlier discussions have proven that altering the mixing ratio of hybrid nanocoolant could result in distinct heat transfer performance. 7G-3T had the highest Nusselt number, OHTC, and radiator effectiveness of any mixing ratios investigated, followed by 3G-7T, 5G-5T, and 10G.

3.4 Correlations for Heat Transfer Performance

One hundred forty-four sets of experimental data resulting from the combinations of air velocity, nanoparticles concentration, and Reynolds number were used to generate correlations for hybrid nanocoolant with a mixing ratio of 7G-3T. In this study, correlations were developed using Minitab 18 software for estimating both tube side OHTC and radiator effectiveness from the variation of working parameters. Based on all illustrations in previous sections, a non-linear relationship was

observed between responses (OHTC and effectiveness) and working parameters. Hence, response surface methodology (RSM) was adopted to optimize the data obtained in full factorial matrix and generate regression models to estimate the heat transfer performance of hybrid nanocoolant used in this study.

$$U_{in,est} = -18.3 + 641 w_{np} + 93.9 v_{air} + 0.7516\,\mathrm{Re} - 4125 w_{np}^{\ 2} \\ -0.001987\,\mathrm{Re}^2 + 274.9 w_{np} \cdot v_{air} + 1.654 w_{np} \cdot \mathrm{Re} + 0.2843 v_{air} \cdot \mathrm{Re} \quad (27)$$

$$\varepsilon_{est} = 0.1415 + 0.94 w_{np} - 0.00189 v_{air} + 0.002094\,\mathrm{Re} - 3.065 w_{np}^{\ 2} \\ -0.000004\,\mathrm{Re}^2 + 0.000939 w_{np} \cdot \mathrm{Re} + 0.000103 v_{air} \cdot \mathrm{Re} \quad (28)$$

Based on the equations above, weightage concentration of nanoparticles ($0.025 \leq \omega_{np} \leq 0.1$ wt.%), inlet velocity of cooling air ($1.7 \leq v_{air} \leq 1.9$ m/s), and coolant Reynolds number ($40.4 \leq \mathrm{Re} \leq 317.5$) were inserted directly into the regressions without any unit conversion. The developed correlations were only valid for coolant inlet temperature of 35 ^{o}C. The subscript est indicates estimated performance.

Figure 14 illustrates the reliability of proposed correlations based on a comparison of experimental results and predicted values. The maximum deviation obtained was only 3.95% and 7.17% for estimating tube side OHTC and radiator effectiveness, respectively. The excellent agreement (< 10%) with experimental data hence validated the proposed correlations.

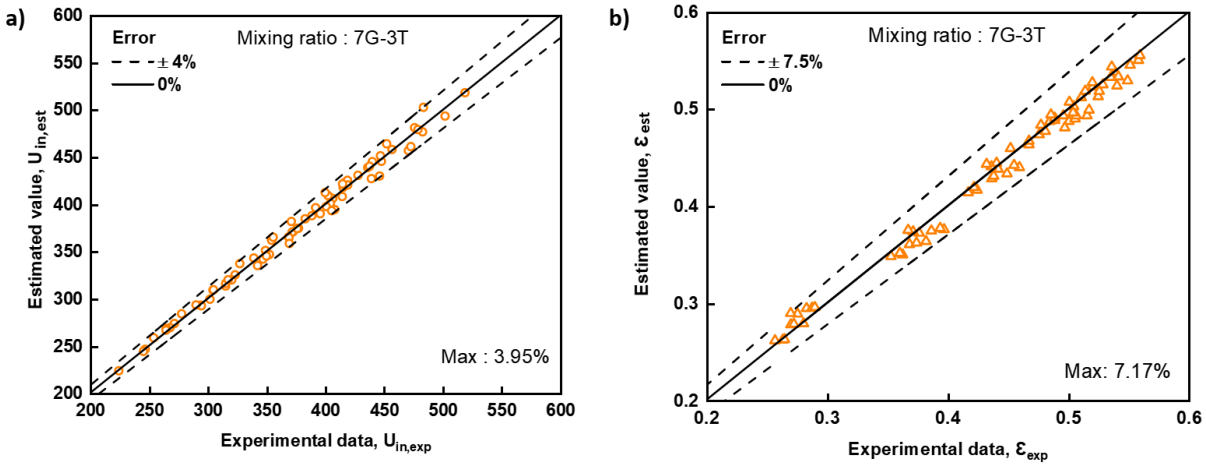

Figure 14. Comparison of estimated heat transfer performance against experimental data. a) Tube side OHTC b) Effectiveness of radiator

4.0 Conclusion

The significance of a less-focused parameter in previous studies - the mixing ratio of hybrid nanocoolant - was reported in this work. Its impact on heat transfer performance was discussed, and accurate correlations were proposed. The main findings of this work can be summarised as follows:

1. The Nusselt number computed in the present research agreed well with Dehghandokht's and Shah-London's correlations. Both the air and tube side heat transfer rates showed acceptable heat balance error.

2. Air velocity had a slight effect on heat transfer enhancement. Reynolds number and nanoparticle concentration were far more dominant.

3. A nanocoolant with a mixing ratio of 7G-3T demonstrated the most heat transfer augmentation across all tested conditions. For both heat transfer performance indicators, nanocoolant with mixing ratios of 10G and 5G-5T showed deterioration at nanoparticle concentration of 0.025 wt.% and 0.05 wt.%, respectively, in most testing conditions.

4. Compared to the base coolant, the maximum increment in Nusselt number, overall heat transfer coefficient, and radiator effectiveness were 4.94%, 35.87%, and 20.48%, respectively.

5. A higher ratio of highly conductive material did not improve thermal performance. It is most likely due to the smaller particles intercalating between the GnP sheets. The suggested mixing ratio of CGnP-TiO_2 nanocomposite for high thermal performance is 7G-3T > 3G-7T > 5G-5T $\geq$ 10G.

Acknowledgement

The authors would like to thank Universiti Teknologi Malaysia for funding the study's materials and equipment through the Takasago research grant (R.K130000.7843.5F273).

References

1. Nasef, H., S. Nada, and H. Hassan, *Integrative passive and active cooling system using PCM and nanofluid for thermal regulation of concentrated photovoltaic solar cells.* Energy Conversion and Management, 2019. **199**: p. 112065.

2. Boyaghchi, F.A. and M. Chavoshi, *Monthly assessments of exergetic, economic and environmental criteria and optimization of a solar micro-CCHP based on DORC.* Solar Energy, 2018. **166**: p. 351-370.
3. Zangeneh, A., et al., *Experimental study of forced convection and subcooled flow boiling heat transfer in a vertical annulus using different novel functionalized ZnO nanoparticles.* Applied Thermal Engineering, 2016. **109**: p. 789-802.
4. Bashar, M. and K. Siddiqui, *Experimental investigation of transient melting and heat transfer behavior of nanoparticle-enriched PCM in a rectangular enclosure.* Journal of Energy Storage, 2018. **18**: p. 485-497.
5. Choi, S.U. and J.A. Eastman, *Enhancing thermal conductivity of fluids with nanoparticles*. 1995, Argonne National Lab., IL (United States).
6. Gulhane, A. and S. Chincholkar, *Experimental investigation of convective heat transfer coefficient of Al2O3/water nanofluid at lower concentrations in a car radiator.* Heat Transfer—Asian Research, 2017.
7. Sheikhzadeh, G., M. Fakhari, and H. Khorasanizadeh, *Experimental Investigation of Laminar Convection Heat Transfer of Al2O3-Ethylene Glycol-Water Nanofluid as a Coolant in a Car Radiator*. Journal of Applied Fluid Mechanics, 2017. **10**(1): p. 209-219.
8. Subhedar, D.G., B.M. Ramani, and A. Gupta, *Experimental investigation of heat transfer potential of Al2O3/Water-Mono Ethylene Glycol nanofluids as a car radiator coolant.* Case studies in thermal engineering, 2018. **11**: p. 26-34.
9. Elsaid, A.M., *Experimental study on the heat transfer performance and friction factor characteristics of Co3O4 and Al2O3 based H2O/(CH2OH) 2 nanofluids in a vehicle engine radiator.* International Communications in Heat and Mass Transfer, 2019. **108**: p. 104263.
10. Jagadishwar, K. and S. Sudhakar Babu, *Performance investigation of water and propylene glycol mixture based nano-fluids on automotive radiator for enhancement of heat transfer.* International Journal of Mechanical Engineering and Technology, 2017. **8**(7): p. 822-833.
11. Devireddy, S., C.S.R. Mekala, and V.R. Veeredhi, *Improving the cooling performance of automobile radiator with ethylene glycol water based TiO 2 nanofluids.* International Communications in Heat and Mass Transfer, 2016. **78**: p. 121-126.
12. Zhou, X., et al., *Comparison of heat transfer performance of ZnO-PG, α-Al2O3-PG, and γ-Al2O3-PG nanofluids in car radiator.* Nanomaterials and Nanotechnology, 2019. **9**: p. 1847980419876465.
13. Zhou, M., et al., *Analysis of flow and heat transfer characteristics of micro-pin fin heat sink using silver nanofluids.* Science China Technological Sciences, 2012. **55**(1): p. 155-162.
14. Kaggwa, A., et al., *The effect of surfactants on viscosity and stability of activated carbon, alumina and copper oxide nanofluids.* Materials Today: Proceedings, 2019. **18**: p. 510-519.
15. Tafakhori, M., et al., *Assessment of Fe 3 O 4–water nanofluid for enhancing laminar convective heat transfer in a car radiator.* Journal of Thermal Analysis and Calorimetry, 2020: p. 1-13.
16. Oliveira, G.A., E.M.C. Contreras, and E.P. Bandarra Filho, *Experimental study on the heat transfer of MWCNT/water nanofluid flowing in a car radiator.* Applied Thermal Engineering, 2017. **111**: p. 1450-1456.
17. Said, Z., et al., *Enhancing the performance of automotive radiators using nanofluids.* Renewable and Sustainable Energy Reviews, 2019. **112**: p. 183-194.
18. Palaniappan, B. and V. Ramasamy, *Thermodynamic analysis of fly ash nanofluid for automobile (heavy vehicle) radiators.* Journal of Thermal Analysis and Calorimetry, 2019. **136**(1): p. 223-233.
19. Soylu, S.K., et al., *Improving heat transfer performance of an automobile radiator using Cu and Ag doped TiO2 based nanofluids.* Applied Thermal Engineering, 2019. **157**: p. 113743.
20. Kumar, V. and R.R. Sahoo, *Exergy and energy performance for wavy fin radiator with a new coolant of various shape nanoparticle-based hybrid nanofluids.* Journal of Thermal Analysis and Calorimetry, 2020: p. 1-12.
21. Sahoo, R.R., *Heat transfer and second law characteristics of radiator with dissimilar shape nanoparticle-based ternary hybrid nanofluid.* Journal of Thermal Analysis and Calorimetry, 2020: p. 1-13.
22. Asokan, N., P. Gunnasegaran, and V.V. Wanatasanappan, *Experimental investigation on the thermal performance of compact heat exchanger and the rheological properties of low concentration mono and hybrid nanofluids containing Al2O3 and CuO nanoparticles.* Thermal Science and Engineering Progress, 2020. **20**: p. 100727.
23. Vermahmoudi, Y., et al., *Experimental investigation on heat transfer performance of Fe2O3/water nanofluid in an air-finned heat exchanger.* European Journal of Mechanics-B/Fluids, 2014. **44**: p. 32-41.
24. Topuz, A., et al., *Experimental investigation of pressure drop and cooling performance of an automobile radiator using Al 2 O 3-water+ ethylene glycol nanofluid.* Heat and Mass Transfer, 2020. **56**(10): p. 2923-2937.
25. Barzegarian, R., A. Aloueyan, and T. Yousefi, *Thermal performance augmentation using water based Al2O3-gamma nanofluid in a horizontal shell and tube heat exchanger under forced circulation.* International Communications in Heat and Mass Transfer, 2017. **86**: p. 52-59.
26. Jafari, S.M., et al., *Heat Transfer Enhancement in Thermal Processing of Tomato Juice by Application of Nanofluids.* Food and Bioprocess Technology, 2017. **10**(2): p. 307-316.
27. Darzi, A.A.R., M. Farhadi, and K. Sedighi, *Heat transfer and flow characteristics of AL2O3–water nanofluid in a double tube heat exchanger.* International Communications in Heat and Mass Transfer, 2013. **47**: p. 105-112.

28. Duangthongsuk, W. and S. Wongwises, *An experimental study on the heat transfer performance and pressure drop of TiO2-water nanofluids flowing under a turbulent flow regime.* International Journal of Heat and Mass Transfer, 2010. **53**(1): p. 334-344.
29. Raei, B., et al., *Experimental study on the heat transfer and flow properties of γ-Al2O3/water nanofluid in a double-tube heat exchanger.* Journal of Thermal Analysis and Calorimetry, 2017. **127**(3): p. 2561-2575.
30. Hung, Y.-H., et al., *Performance evaluation of an air-cooled heat exchange system for hybrid nanofluids.* Experimental Thermal and Fluid Science, 2017. **81**: p. 43-55.
31. Ravi Kumar, N.T., et al., *Heat transfer, friction factor and effectiveness of Fe3O4 nanofluid flow in an inner tube of double pipe U-bend heat exchanger with and without longitudinal strip inserts.* Experimental Thermal and Fluid Science, 2017. **85**: p. 331-343.
32. Selvam, C., et al., *Convective heat transfer characteristics of water–ethylene glycol mixture with silver nanoparticles.* Experimental Thermal and Fluid Science, 2016. **77**: p. 188-196.
33. Contreras, E.M.C., G.A. Oliveira, and E.P. Bandarra Filho, *Experimental analysis of the thermohydraulic performance of graphene and silver nanofluids in automotive cooling systems.* International Journal of Heat and Mass Transfer, 2019. **132**: p. 375-387.
34. Palanisamy, K. and P.C.M. Kumar, *Heat transfer enhancement and pressure drop analysis of a cone helical coiled tube heat exchanger using MWCNT/water nanofluid.* Journal of Applied Fluid Mechanics, 2017. **10**(SpecialIssue): p. 7-13.
35. Nieh, H.-M., T.-P. Teng, and C.-C. Yu, *Enhanced heat dissipation of a radiator using oxide nano-coolant.* International Journal of Thermal Sciences, 2014. **77**: p. 252-261.
36. Bhattad, A., J. Sarkar, and P. Ghosh, *Heat transfer characteristics of plate heat exchanger using hybrid nanofluids: effect of nanoparticle mixture ratio.* Heat and Mass Transfer, 2020: p. 1-16.
37. Ma, M., et al., *Synergistic mechanism of thermal conductivity enhancement and economic analysis of hybrid nanofluids.* Powder Technology, 2020. **373**: p. 702-715.
38. Hamid, K.A., et al., *Experimental investigation of nanoparticle mixture ratios on TiO2–SiO2 nanofluids heat transfer performance under turbulent flow.* International Journal of Heat and Mass Transfer, 2018. **118**: p. 617-627.
39. Xian, H.W., N.A.C. Sidik, and R. Saidur, *Impact of different surfactants and ultrasonication time on the stability and thermophysical properties of hybrid nanofluids.* International Communications in Heat and Mass Transfer, 2020. **110**: p. 104389.
40. Devireddy, S., C.S.R. Mekala, and V.R. Veeredhi, *Improving the cooling performance of automobile radiator with ethylene glycol water based TiO2 nanofluids.* International communications in heat and mass transfer, 2016. **78**: p. 121-126.
41. Sheikhzadeh, G., M. Fakhari, and H. Khorasanizadeh, *Experimental investigation of laminar convection heat transfer of Al2O3-ethylene glycol-water nanofluid as a coolant in a car radiator.* J. Appl. Fluid Mech, 2017. **10**(1): p. 209-219.
42. Kumar, V. and R.R. Sahoo, *Exergy and energy performance for wavy fin radiator with a new coolant of various shape nanoparticle-based hybrid nanofluids.* Journal of Thermal Analysis and Calorimetry, 2021. **143**(6): p. 3911-3922.
43. Qasim, M., et al., *Heat Transfer Enhancement of an Automobile Engine Radiator using ZnO Water Base Nanofluids.* Journal of Thermal Science, 2020. **29**(4): p. 1010-1024.
44. Alosious, S., et al., *Experimental and numerical study on heat transfer enhancement of flat tube radiator using Al 2 O 3 and CuO nanofluids.* Heat and Mass Transfer, 2017. **53**(12): p. 3545-3563.
45. El Bécaye Maïga, S., et al., *Heat transfer enhancement by using nanofluids in forced convection flows.* International Journal of Heat and Fluid Flow, 2005. **26**(4 SPEC. ISS.): p. 530-546.
46. Dehghandokht, M., et al., *Flow and heat transfer characteristics of water and ethylene glycol-water in a multi-port serpentine meso-channel heat exchanger.* International Journal of Thermal Sciences, 2011. **50**(8): p. 1615-1627.
47. Shah, R. and A. London, *Advances in heat transfer.* Laminar Forced Flow Convection in Ducts, Suppl, 1978. **1**.
48. Sieder, E.N. and G.E. Tate, *Heat transfer and pressure drop of liquids in tubes.* Industrial & Engineering Chemistry, 1936. **28**(12): p. 1429-1435.
49. Siddiqui, F.A., E.S. Dasgupta, and A. Fartaj, *Experimental investigation of air side heat transfer and fluid flow performances of multi-port serpentine cross-flow mesochannel heat exchanger.* International journal of heat and fluid flow, 2012. **33**(1): p. 207-219.
50. Sieder, E.N. and G.E. Tate, *Heat Transfer and Pressure Drop of Liquids in Tubes.* Industrial and Engineering Chemistry, 1936. **28**(12): p. 1429-1435.
51. Moffat, R.J., *Describing the uncertainties in experimental results.* Experimental Thermal and Fluid Science, 1988. **1**(1): p. 3-17.
52. Ali, M., A. El-Leathy, and Z. Al-Sofyany, *The effect of nanofluid concentration on the cooling system of vehicles radiator.* Advances in Mechanical Engineering, 2014. **6**: p. 962510.

53. Khan, A., et al., *Experimental investigation of enhanced heat transfer of a car radiator using ZnO nanoparticles in H 2 O–ethylene glycol mixture*. Journal of Thermal Analysis and Calorimetry, 2019. **138**(5): p. 3007-3021.
54. Selvam, C., et al., *Overall heat transfer coefficient improvement of an automobile radiator with graphene based suspensions.* International Journal of Heat and Mass Transfer, 2017. **115**: p. 580-588.